Journal of Polymers and the Environment (2018) 26:3937–3948
https://doi.org/10.1007/s10924-018-1269-5

ORIGINAL PAPER

Environmentally Friendly Chitosan-g-poly(acrylic acid-*co*-acrylamide)/Ground Basalt Superabsorbent Composite for Agricultural Applications

Majd Said[1] · Yomen Atassi[1] · Mohammad Tally[1] · Hany Khatib[1]

Published online: 21 June 2018

Abstract
This paper investigates on the preparation of a novel eco-friendly composite hydrogel, chitosan-g-poly(acrylic acid-*co*-acrylamide)/ground basalt and its potential application as a soil ameliorant. Synthesis was undergone using microwave irradiation. *N,N′*-methylene bisacrylamide MBA was used as a cross-linker, whereas potassium peroxydisulfate KPS and *N,N,N′,N′*-tetramethylene diamine TEMED were used as radical initiator and reaction accelerator, respectively. The incorporation of ground basaltic rocks into the hydrogel was very beneficial: (i) It lowers the cost of the final hydrogel, (ii) It enhances the mechanical strength of the hydrogel, (iii) It boosts the maximum water absorbency of the composite, 650 g/g versus 450 g/g for the hydrogel without basalt and (iv) It promotes the thermal stability of the composite in comparison with the hydrogel alone. The prepared composite hydrogel was characterized by FTIR, X-ray diffractometer and scanning electron microscope SEM. The effects of pH and ionic strength on water absorbency were also investigated. The role of the prepared composite as a soil conditioner is performed using eggplant (*Solanum melongena*) as a model.

Keywords Chitosan · Superabsorbent polymers · Polyacrylate · Polyacrylamide · Soil ameliorant · Basalt

Introduction

With the increase of world population, food security and freshwater sustainability become at risk [1]. To cope with food insecurity and address the challenges of water scarcity, extensive efforts should be done to improve the efficiency of water use, especially in arid and semi-arid regions [2, 3]. Investigations on new materials that help in increasing soil fertility and reduce irrigation frequency have recently received great attention [4]. Superabsorbent hydrogels (SAHs) are promising candidates to address these issues. They are water swellable, slightly cross-linked polymeric network that can absorb great amounts water and retain it even under some pressure [5–8]. They are usually administered to the soil as granules that swell after soil watering and release it to plant roots when the soil gets dry. In this way, the risk of water loss by evaporation and drainage is restrained [3]. Furthermore, the incorporation of fertilizers and nutrients inside SAHs network structure and their subsequent gradual release are quite possible [2, 9]. However, common SAHs are prepared from acrylic monomers which are expensive, non-biodegradable and synthesized from non-renewable resources [10, 11]. When designing novel SAHs, some criteria are taken into considerations such as: high water absorption, fast absorption rate, biodegradability, cost-effectiveness and good mechanical strength [12, 13]. In this regard, intensive research has been conducted on the use of renewable and environment friendly resources to prepare multicomponent SAHs by graft polymerization of vinyl monomers on the backbone of biodegradable polymers, such as sodium alginate, carboxymethyl cellulose, starch, chitosan, to name a few [14–16]. In order to improve the mechanical strength of the hydrogels and to lower their production costs, clay based hydrogels using bentonite, attapulgite, diatomite…. have been prepared with/without biodegradable polymers [2, 4, 17–21].

Electronic supplementary material The online version of this article (https://doi.org/10.1007/s10924-018-1269-5) contains supplementary material, which is available to authorized users.

✉ Yomen Atassi
yomen.atassi@hiast.edu.sy

[1] Laboratory of Materials Sciences, Department of Applied Physics, Higher Institute for Applied Sciences and Technology, P.O. Box 31983, Damascus, Syria

To the best of the authors' knowledge, there is no study dealing with the incorporation of ground basaltic rocks into SAH's network. Furthermore, basalt (BT) plays an important role in soil management and has some advantage over soluble fertilizers that provide plants with three macronutrients, namely, nitrogen, phosphorous and potassium [1]. However, common fertilizers do not provide micronutrients contrary to many rocks that contain a multitude of nutrients, including micronutrients [1]. Basalt as a fine grained volcanic rock is considered to be a multinutrient silicate rock fertilizer [22]. It is source for iron, calcium and potassium. Many studies illustrated the beneficial effects of the application of ground basaltic rocks on nutrient depleted soil as it has the potential to supply the soil with a large array of macro and micronutrients in comparison to soluble fertilizers [22, 23]. It is also considered as a slow release fertilizer. In addition, it can raise the pH of affected soil and provides a long-term addition of nutrients like Fe, Ca and K [24].

On the other hand, chitosan (CTS) is the *N*-deacetylated derivative of chitin, a linear poly-β-(1,4)-*N*-acetyl-D-glucosamine and one of the most abundant natural biopolymer in the world. It is ranked as the second in abundance behind only cellulose. Chitosan is produced by *alkaline* deacetylation of chitin extracted from exoskeletons of crustaceans [25].

This study deals with the incorporation of ground basaltic rock, as a soil ameliorant, to a hydrogel based on chitosan biopolymer grafted onto poly(acrylic acid-*co*-acrylamide): CTS-g-P(AA-*co*-AM)/BT under microwave irradiation. This brand-new hydrogel composite combines chitosan with basalt to create a cost-effective and environment friendly soil conditioner intended to boost the growth of plants. Eggplant (*Solanum melongena*) was selected as an example to illustrate this effect. Structural and morphological characterization of the composite were performed using FTIR spectroscopy, X-ray diffractometry and scanning electron microscopy, SEM. Effect of environmental conditions such as pH of the medium and the ionic strength on water absorbency are also investigated. The quantities of chitosan and ground basalt were optimized to get maximum water absorbency with good mechanical strength of the hydrogel.

Experimental

Chemicals and Materials

Chitosan (CTS, from Sigma-Aldrich, (75–85)% degree of deacetylation and medium average molecular weight, viscosity 200–800 cps). Acrylic acid (AA) and Acrylamide (AM), for synthesis, were from Merck and they are used as purchased. Potassium peroxydisulfate (KPS), GR for analysis, as an initiator, *N,N′*-methylene bisacrylamide (MBA), special grade for molecular biology, as a cross-linked, and *N,N,N′,N′*-tetramethylene diamine (TEMED) GR for analysis as an accelerator are also obtained from Merck. Sodium hydroxide NaOH micro granular pure (POCH) is used for acid neutralization. Solvents: methanol and ethanol (GR for analysis) are obtained from Merck. Sodium chloride (NaCl), magnesium chloride ($MgCl_2$) and aluminium chloride ($AlCl_3$) are purchased from Merck (GR for analysis). Basalt rocks are obtained from Homs Governorate in Syria (Table 1).

Instrumental Analysis

The FTIR spectra of hydrogels in the 400–4000 cm^{-1} range were recorded at room temperature using infrared spectrophotometer (Bruker, Vector 22). For pellets preparation, powders were dispersed in the KBr and then pressed at 5 tons in a cylindrical die to obtain pellets of around 1 mm thickness. X-ray diffraction patterns were performed with PHILIPS-PW3710X-RAY diffractometer operating at 60 kV using Cu-K_α radiation ($\lambda = 0.154$ nm) in the 2θ range: 10°–60°. Thermogravimetric Analyses of hydrogels were performed using SETARAM, Labsys TG, TG-DSC 1600 °C, from room temperature to 600 °C at a heating rate of 10 °C/min and under argon atmosphere. The morphology of the samples was examined using scanning electron microscope VEGA II TESCAN, SEM instrument. The samples were coated with graphite.

Swelling Measurements

Measurements of water absorbency of hydrogel samples are performed by the free swelling method. Water absorbency is estimated in grams of water per one gram of the hydrogel. An accurately weighed amount of the investigated hydrogel (ca. 0.1 g) is submerged in 500 mL of distilled water at room temperature for at least 4 h. Then, the swollen hydrogel is filtered through weighed 100-mesh sieve (pore size150 μm) until no water drops out. The mass of the swollen hydrogel is measured

Table 1 Elemental analysis of basalt

K_2O	Al_2O_3	Mn_2O_3	Cr_2O_3	CaO	Fe_2O_3	MgO	Na_2O	SiO_2	P_2O_5
0.93	14.78	0.2	0.3	10.96	14.64	6.17	2.91	46.01	0.53

after draining, and water absorbency is evaluated using the following Eq. (1):

$$S_{eq} = (w_s - w_d)/w_d \quad (1)$$

where S_{eq} is the equilibrium water absorbency in grams of water per gram of hydrogel sample; w_d and are the masses of the dried and swollen hydrogel sample, respectively [26, 27].

Gel Content

Gel content is evaluated by dispersing an accurately weighed dried sample of the hydrogel in distilled water until it swells completely. Then, the swollen sample is filtered and washed with distilled water several times. The sample is dewatered in excess ethanol for 48 h, and dried at 50 °C for 12 h until the sample has a constant weight. The gel content is defined using the following equation [28].

$$\text{Gel}(\%) = \frac{w_d}{w_i} \times 100 \quad (2)$$

where w_d is the mass of dried hyrogel after extraction and w_i is the initial mass of the hydrogel.

Grafting Percentage and Grafting Efficiency

The evaluation of grafting percentage (G%) and the grafting efficiency (E%) is performed using Eqs. 1, 4 [29–31]:

$$\text{G}\% = \frac{w_1 - w_0}{w_0} \times 100 \quad (3)$$

$$\text{E}\% = \frac{w_1 - w_0}{w_2} \times 100 \quad (4)$$

where w_0, w_1, w_2 are the mass of CTS, mass of the hydrogel and mass of the monomers, respectively.

Water Retention

In order to estimate the water retention of the hydrogel sample at constant temperature, the pre-weighed swollen hydgel w_3 equilibrated in distilled water is left at ambient temperature for 24 h. Then, the hydrogel is weighed again w_4. The percentage water retention is estimated using the equation [32]:

$$\text{Water retention}\,(\%) = \frac{w_4}{w_3} \times 100 \quad (5)$$

Swelling Kinetics at Different pH Values

In order to determine the rate of absorbency of the hydrogel at different pH values, accurately weighed quantities (ca. 0.1 g) of the hydrogel is immersed in 500 mL of aqueous solutions at different pH values (pH 3.0, 5.0 and 10.0) at ambient temperature. At consecutive time intervals, the water absorbency of the hydrogel is measured according to the above mentioned method.

Preparation of CTS-g-P(AA-*co*-AM) Hydrogel and Its Composite with Basalt

The hydrogels are synthesized by graft free radical copolymerization of poly(AA-*co*-AM) onto CTS according to the following procedure:

Acrylic acid AA (6 g) is partially neutralized to 75 wt% by NaOH solution (5 M) in an ice bath to avoid polymerization. Then, the acrylic acid solution is added to a solution of acrylamide Am (6 g in ca. 10 mL of distilled water) under continuous stirring. After that, MBA solution (0.05 g in ca. 5 mL of distilled water) is added to monomers solution.

1 g of Chitosan CTS is dissolved in 40 mL of acetic acid solution (2%) under mechanical stirring at 60 °C for 15 min. Two equimolar aqueous solutions of the redox initiator system of KPS, 0.1 g and TEMED, 0.05 g (each dissolved in ca. 5 mL of distilled water) are prepared and then dropwise added to the solution of CTS under vigorous mechanical stirring and kept at 60 °C for 15 min to generate radicals. After cooling this solution to 40 °C, the monomers solution is dropwise added on it, under continuous stirring at 1050 rpm for 15 min. The total volume of the reactive mixture is brought to 100 mL by adding distilled water. Then, the final solution is treated in a microwave oven at the power of 950 W for 60 s. The viscosity of the solution gradually increases and the gelation point is reached after 50 s.

The elastic gel is cut to small pieces. Then, it is washed thoroughly with methanol for several times. After that, it is immersed for 24 h in absolute methanol for dewatering and dissolving non reacting reagent. Finally, it is washed by ethanol, and dried for several hours at 60 °C until it becomes a brittle solid. At this stage, the solid is milled and dried at 60 °C for 24 h.

The composite CTS-g-P(AA-*co*-AM)/BT is prepared in the same way described above, and an optimized amount of (3 g) of basalt is added to chitosan solution after adding the redox system TEMED/KPS adding. The final mixture is treated in a microwave oven at the power of 950 W for 70 s.

Results and Discussions

Synthesis and Mechanistic Aspects

The hydrogels were prepared by free radical by graft polymerization of acrylamide (AM), acrylic acid (AA) onto CTS chain were carried out using the crosslinker (MBA) radical initiator (KPS) and reaction accelerator

(TEMED). Metal and non-metal oxides in ground basalt play the role of physical crosslinking agents that enhance the mechanical strength of the composite hydrogel by intermolecular interactions between the graft copolymer and the basalt oxides. Figure 1 represents a suggested mechanistic pathway of the copolymerization. According to Feng et al., the persulfate ion decomposes upon heating in presence of TEMED to produce hydrogen sulfate anion-radicals that abstract hydrogen atoms from the hydroxyl groups of chitosan to form macro-radicals [33]. The macroradical centers initiate the graft polymerization of acrylic monomers. The presence of crosslinking agent (MBA) leads to a crosslinked structure [34].

Optimization of Chitosan and Basalt Contents in the Composite Hydrogel

The optimized amounts of chitosan and basalt in the hydrogel were determined after an initial screening in which the content of chitosan was varied from 0.5 to 1.2 g, Fig. 1S. The absorption capacity was determined for each quantity of chitosan. With increasing the quantity of chitosan, the grafting

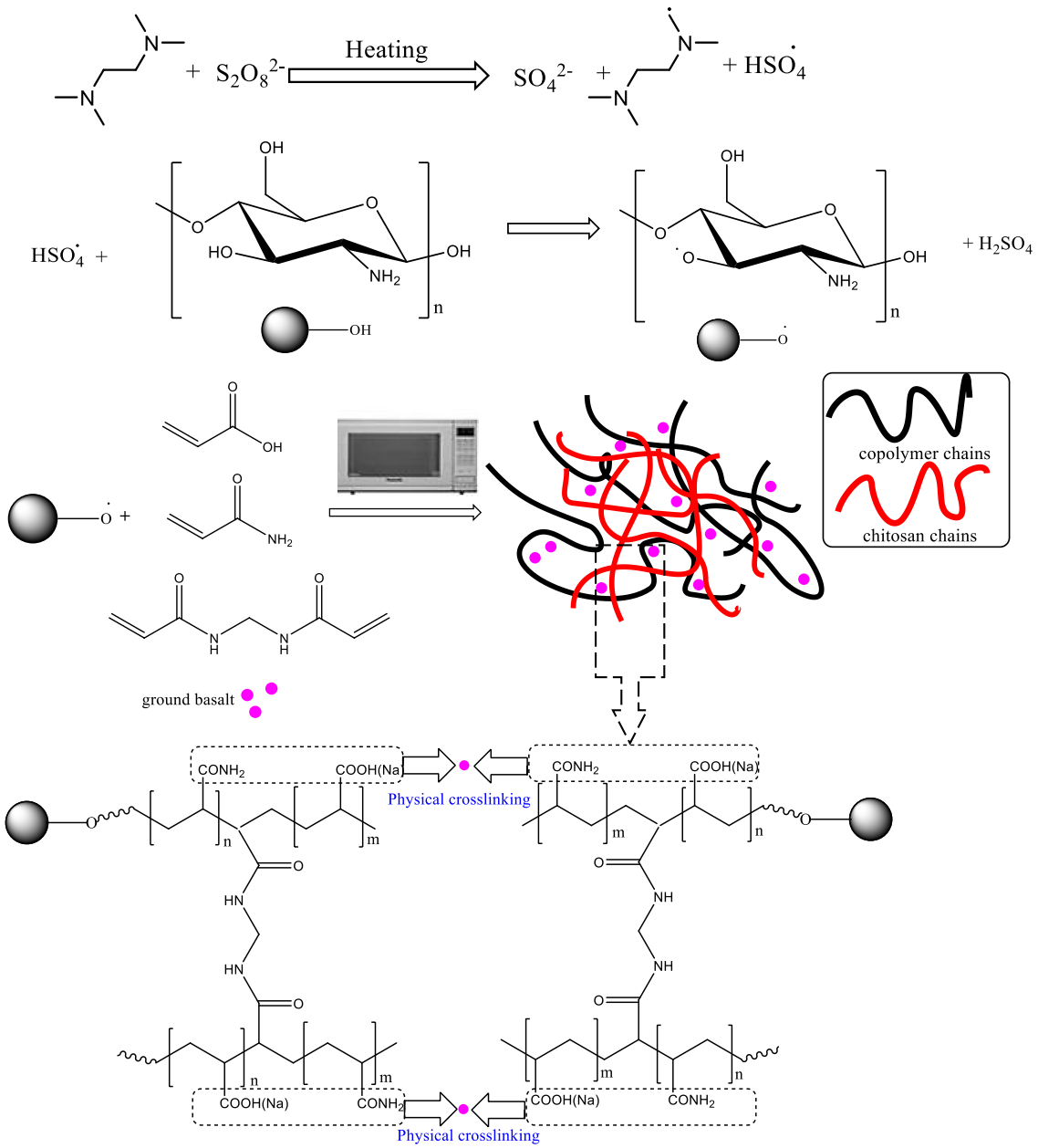

Fig. 1 Schematic mechanistic pathway for the synthesis of CTS-g-P(AA-*co*-AM)/BT composite hydrogel

efficiency increases and the water absorbency increases. However, at a certain value of chitosan, the relatively high viscosity of reaction solution hinders the efficiency of the grafting and the absorption capacity decreases. The highest value of absorption capacity was obtained for the hydrogel containing 1 g of chitosan. Thus, this value for chitosan was employed in the study. On the other hand, the content of basalt was varied from 1 to 3.1 g, Fig. 2S. The highest value for water absorbency without collapse of the hydrogel was when 3 g of basalt is added. Accordingly, this value was used in the current study. The interaction among ground basalt, CTS, and acrylic monomers become gradually intensive with increasing basalt content. In fact, the high repulsive forces between the negative surface charge of basalt and COO^- groups results in increased expansion of the hydrogel network and a higher water absorbency [30, 35]. According to the IR analysis (discussed in "FTIR Spectra" section), the –OH of basalt may participate in the formation of the composite hydrogel, which could improve the polymeric network, and then enhance the water absorbency. With further increase in basalt, more chemical and physical cross-linkages are formed in the polymeric network, and then the elasticity of the polymer chains decreases, which would decrease the water absorbency of the superabsorbent composite [36].

FTIR Spectra

The FTIR spectrum of chitosan is shown in Fig. 2a. The wide band at 3478 cm^{-1} is attributed to the stretching vibration of O–H chemical bond. The peak at 2924 cm^{-1} corresponds to the stretching vibration of C–H. The absorption peaks at 1646 and 1424 cm^{-1} are associated with the C=O stretching of the amide group and bending of the C–H bond, respectively. The band at 1150 cm^{-1} corresponds to antisymmetric stretching of C–O–C bridge.

Figure 2b shows the FTIR spectrum of basalt. The peaks, observed at 3429 and at 1610 cm^{-1}, correspond to the frequency of O–H bond stretching and bending, respectively. The broad band at 1029 cm^{-1} and the peak at 744 cm^{-1} correspond to Si–O–Si asymmetrical and symmetrical stretching, respectively. The peak at 470 cm^{-1} is attributed to the bending frequency of Si-O-Si [37].

The FTIR spectrum of CTS-g-P(AA-*co*-AM) is exhibited in Fig. 2d. The hydrogel CTS-g-P(AA-*co*-AM) is made up of a chitosan backbone with side chains with sodium carboxylate and carboxamide functional groups that are demonstrated by characteristic bands at 1564 and 1673 cm^{-1}, respectively. The strong peak at 1565 cm^{-1} is related to the asymmetric stretching mode of the carbonyl group in the carboxylate anion. This peak is reconfirmed by the presence of another sharp peak at 1402 cm^{-1} that is attributed to the symmetric stretching of the carboxylate anion. The broad band in the range 2550–3500 cm^{-1} is due to O–H stretching bands of alcohol and carboxylic acid groups [38–40].

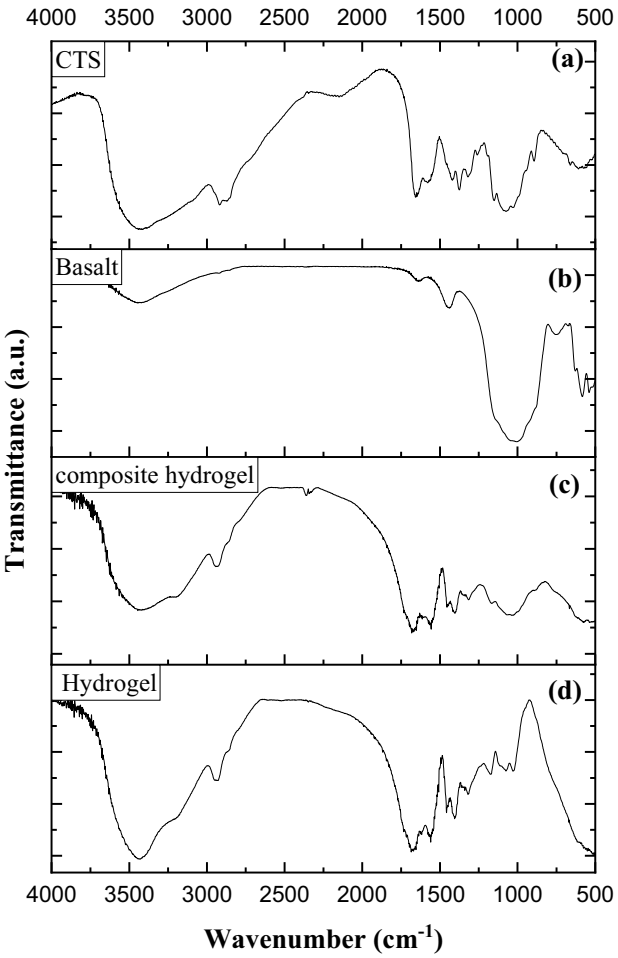

Fig. 2 FTIR spectra of **a** chitosan, **b** basalt, **c** CTS-g-P(AA-*co*-AM)/BT and **d** CTS-g-P(AA-*co*-AM)

To obtain additional evidence of grafting, a similar polymerization is performed in absence of the crosslinker. An appreciable amount of grafted hydrogel was obtained after extracting the homopolymer P(AA-*co*-AM) (8%). The graft copolymer spectrum exhibits identical characteristics to the one of the current study [40].

As for the FTIR spectrum of the novel composite hydrogel CTS-g-P(AA-*co*-AM)/BT, it comprises all the characteristic peaks of both the basalt and CTS-g-P(AA-*co*-AM) with a shift in peaks position towards the red. This indicates the existence of Van der Waals force interactions between the basalt and the CTS-g-P(AA-*co*-AM) hydrogel. Furthermore, the broadening of O–H characteristic bands suggests that basalt may participate in the formation of the composite hydrogel via intermolecular hydrogen bonds, Fig. 2c.

XRD Patterns

X-ray diffraction patterns of the chitosan, the basalt, CTS-g-P(AA-*co*-AM) and CTS-g-P(AA-*co*-AM)/BT are depicted in Fig. 3. The XRD pattern of basalt shows that it is composed of plagioclase (Labradorite) (0.320 and 0.317 nm) and Clinopyroxene (Augite) (0.298 and 0.293 nm) and it is quite similar to the one reported by El-Shahate [37]. The XRD pattern of chitosan exhibits a characteristic peak around 20° [41]. This peak is due to orderly arranged saccharide backbone and inter and intramolecular H-bonding among the hydroxyl and amino groups present on the saccharide units. Upon polymerization, the intensity of the peak is weakened and it becomes broaden owing to the partial destruction of chitosan structure and the reduction in the ability to form hydrogen bonds between hydroxyl and amino groups [42]. The formation of the graft copolymer results in crystallinity destruction of chitosan. One can notice the predominant amorphous nature of the graft copolymer. The reduction in crystallinity may play a primodrial role in influencing hydrogel biodegradability and water absorption capacity. In the composite hydrogel, the characteristic peak of chitosan is also weakened and flattened. The XRD pattern of the composite hydrogel also shows the characteristic peaks of basalt with decreased intensity owing to the deposition of CTS-g-P(AA-*co*-AM) hydrogel on the surfaces of the basalt lattice [30]. Therefore, the XRD analyses suggest that the composite hydrogel consists of CTS-g-P(AA-*co*-AM) amorphous organic phase and crystalline inorganic phase containing basalt [43]. This also indicates the successful synthesis of the CTS-g-P(AA-*co*-AM)/BT hydrogel composite.

Morphological Analyses

SEM micrographs of CTS-g-P(AA-*co*-AM) and CTS-g-P(AA-*co*-AM)/BT hydrogels are depicted in Fig. 4. The

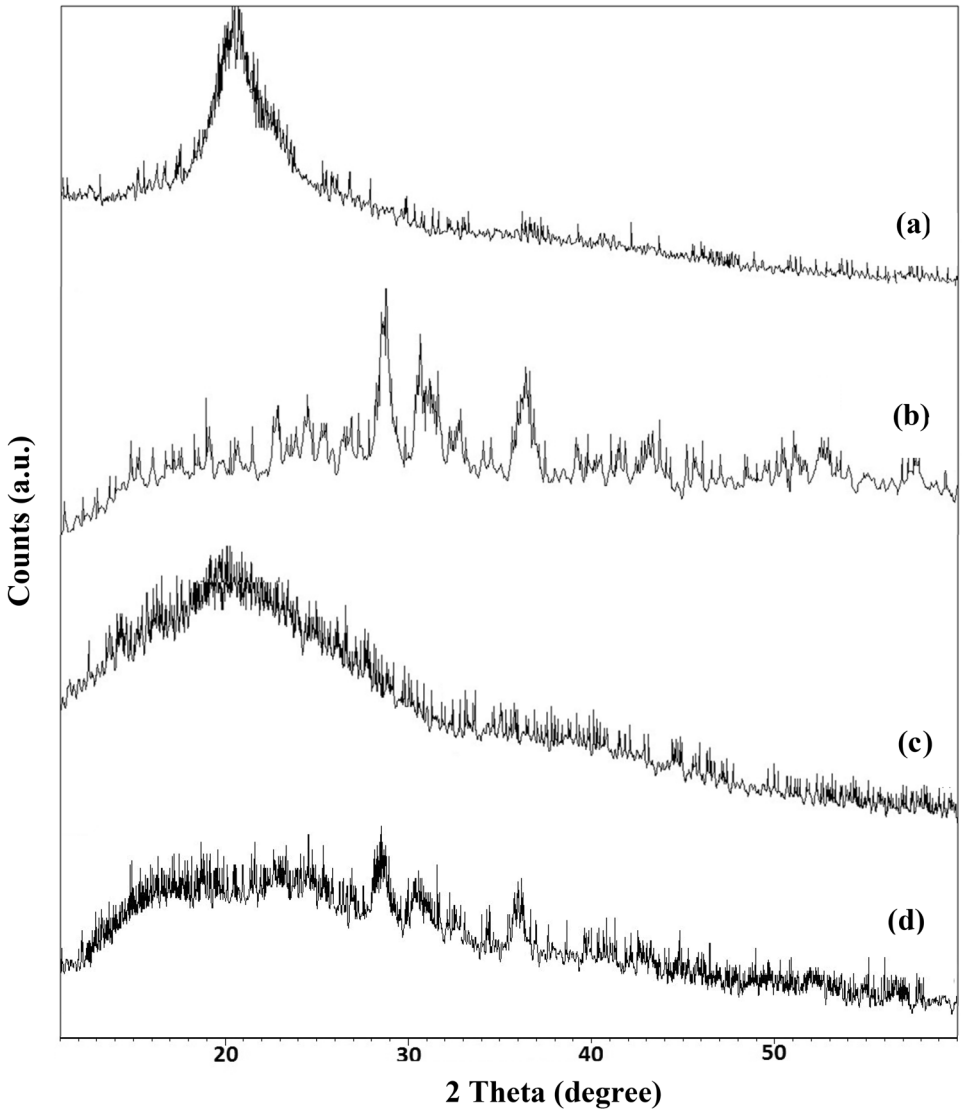

Fig. 3 XRD patterns of (*a*) chitosan, (*b*) basalt, (*c*) CTS-g-P(AA-*co*-AM), (*d*) CTS-g-P(AA-*co*-AM)/BT

micrograghs prove that the hydrogels have porous structure. The globular white objects in CTS-g-P(AA-*co*-AM)/BT micrographs are related to the presence of basalt particles. The main features of micrographs for both hydrogels are the spongy aspects with interconnected pores, since they are semi-open to open cells. The fact that the pores are interconnected enhances hydrogel swelling rate as will be proved in swelling kinetics section [44]. The pore diameters are performed using ImagJ software. It is in the range of 2–5 µm, indicating that SAH belongs to macroporous hydrogels [45]. The porous structure of the as-prepared hyrogels could be linked to the specificity of microwave heating process that induces shorter gelation time (not exceeding 60 s) and more progeny bubbles trapped in the viscous reaction mixture which result in hydrogels with higher porosity [46]. In fact, during the reaction in the microwave oven, the reactive mixture becomes jelly or pasty, which hinders the total removal of the evolved water vapors from the pasty medium. Eventually, the removed vapors create spongy interconnected pores in the gel [47].

Thermogravimetric Analysis

Figure 3S shows the thermogravimetric degradation curves of the basalt, CTS-g-P(AA-*co*-AM) and the composite hydrogel CTS-g-P(AA-*co*-AM)/BT.

Basalt thermogram exhibits a quasi-thermal stability when heating the sample up to 700 °C. However, the thermographs of both CTS-g-P(AA-*co*-AM) and its composite with basalt exhibit two-step degradation behavior. For CTS-g-P(AA-*co*-AM) hydrogel, the first step is in the range 20–270 °C, and is ascribed to the elimination of free and bound water adsorbed to the hydrogel. The onset temperature of the second step starts at 320 °C and is assigned to a thermal decomposition of the hydrogel and formation of volatile compounds such as water vapor, CO_2, NH_3 and CH_4. One should notice that the onset temperature of the thermal decomposition of CTS-g-P(AA- co-AM)/BT, 450 °C, is significantly higher than that of CTS-g-P(AA-*co*-AM). The thermogravimetric analysis indicates that the composite hydrogel exhibits better thermal stability than the hydrogel without basalt. This suggests that the basalt plays the role of heat barrier that hinders the diffusion of volatile products produced during the decomposition process [48]. This can also be confirmed by the temperature of 50% weight loss of the hydrogel without basalt, 375 °C versus 535 °C for CTS-g-P(AA-*co*-AM)/BT.

Water Retention, Gel Content, Grafting Percentage and Grafting Efficiency

Water retention, gel content, grafting efficiency and grafting percentage are calculated for CTS-g-P(AA-*co*-AM) and its basalt composite according to the procedures mentioned in "Experimental" section and the Eqs. 2–5, Table 2. The results indicate that introducing basalt into the hydrogel enhances its water retention making it an efficient water saving material for agriculture application. However, the grafting percentage (G%) and the grafting efficiency (E%) are slightly smaller for the composite hydrogel. This could be attributed to the presence of ground basalt particles within the reactive medium that would hinder the efficiency of the grafting process between the reactants.

Effect of Particle Size on Water Absorption and Water Retention

Figure 5 and 4S(a, b) depict the effects of particle size on water absorbency and water retention of CTS-g-P(AA-*co*-AM) hydrogel and its composite CTS-g-P(AA-*co*-AM)/BT. The particle sizes were varying in the range from 180 µm to more than 425 µm. It can be noted that water retention increases with increasing particle size, whereas water absorbency decreases. These results are associated with smaller specific surface of higher particle size, which promotes water retention but doesn't favor high water absorbency.

Effect of Ionic Strength on Water Absorbency

CTS-g-P(AA-*co*-AM) and its composite with basalt, CTS-g-P(AA-*co*-AM)/BT were examined for the effect of water salinity on their water absorption capacities.

To this end, different concentrations of NaCl, $MgCl_2$ and $AlCl_3$ solutions were prepared to test the effect of ion charge and ion concentration on water absorption capacity.

Figure 5S(a, b) shows that water absorption capacity increases with decreasing the ionic strength of the saline solution. This result obeys to Flory equation [45]. The ionic strength of the solution depends on both the concentration and the charge of each individual ion. The presence of ions in the solution decreases the difference of osmotic pressure between the gel and the solution and consequently the swelling of the gel decreases Moreover, multivalent cations, such as Mg^{2+} and Al^{3+} neutralize several charges inside the gel and can form complex with carboxamide or carboxylate groups. This leads to higher crosslinking degree and consequently loss of swelling.

Effect of pH on Water Absorbency and pH Responsive Characteristics

It is well admitted that water absorption capacity of hydrogels is sensitive to pH values of the medium [49]. In this respect, the swelling of CTS-g-P(AA-*co*-AM) and its composite with basalt is studied at various pH values varied between 1.0 and 12.0 at room temperature, Fig. 6. In this

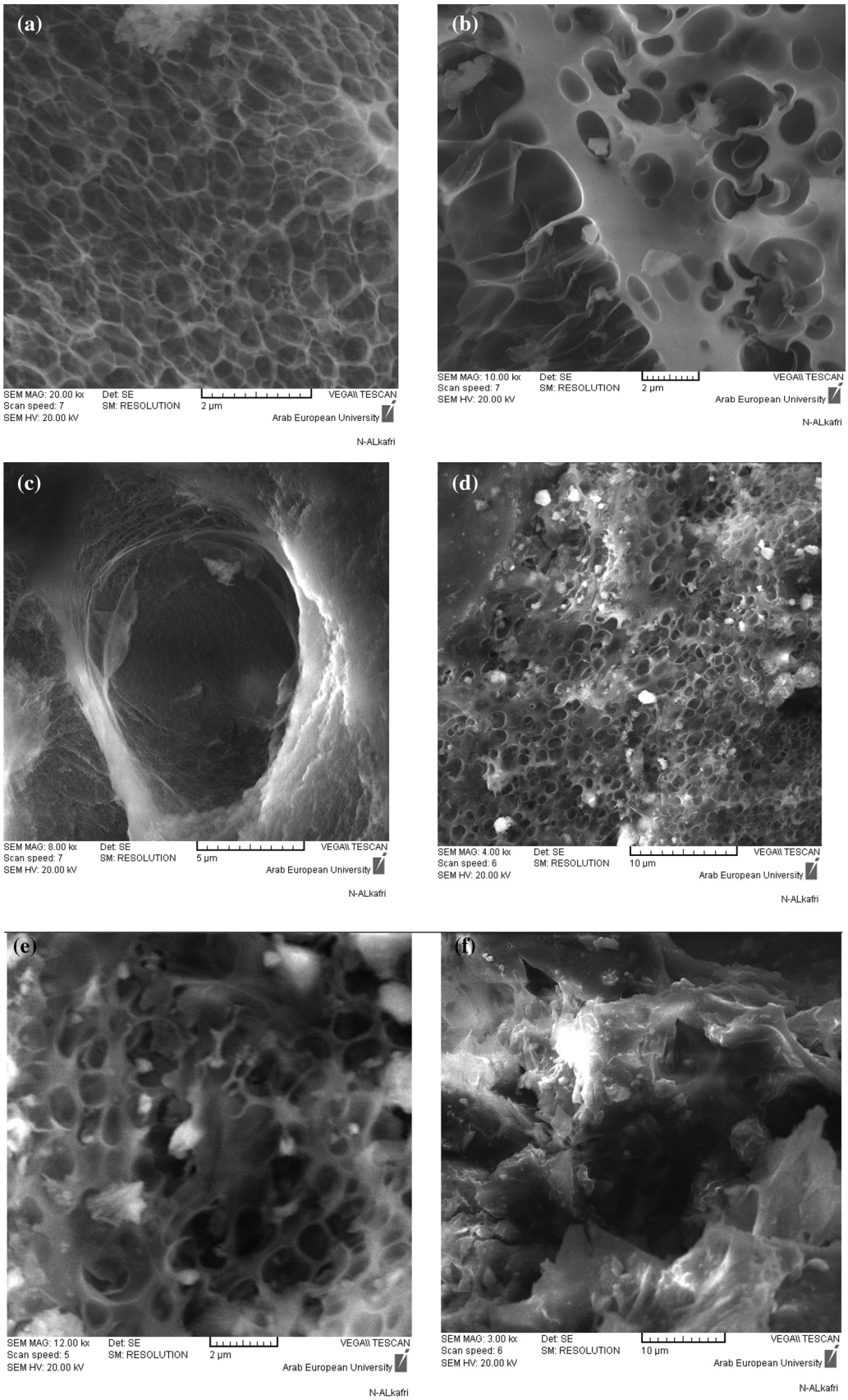

Fig. 4 SEM micrographs of **a**–**c** CTS-g-P(AA-*co*-AM) and **d**–**f** CTS-g-P(AA-*co*-AM)/BT hydrogels at different magnification scales

Table 2 Values of water retention, gel content, grafting percentage and grafting efficiency of CTS-g-P(AA-*co*-AM) and CTS-g-P(AA-*co*-AM)/BT

Sample	Water retention (%)	Gel content (%)	Grafting percentage (G%)	Grafting efficiency (E%)
CTS-g-P(AA-*co*-AM)	89.5	91	1083	90.25
CTS-g-P(AA-*co*-AM) /BT	94	86	976	81.3

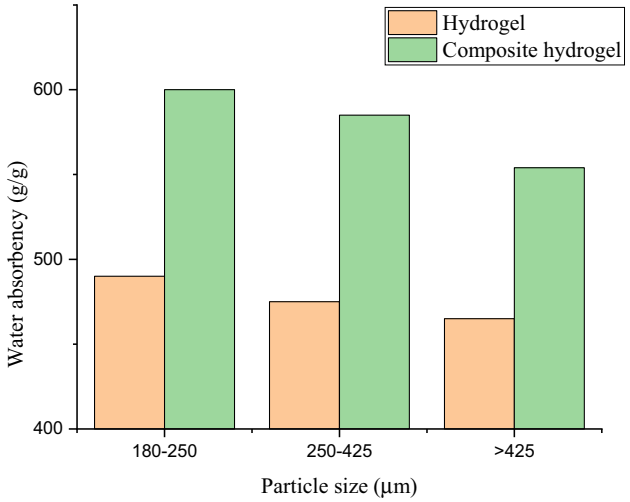

Fig. 5 Effect of particle size on water absorbency for **a** CTS-g-P(AA-*co*-AM) and **b** CTS-g-P(AA-*co*-AM)/BT

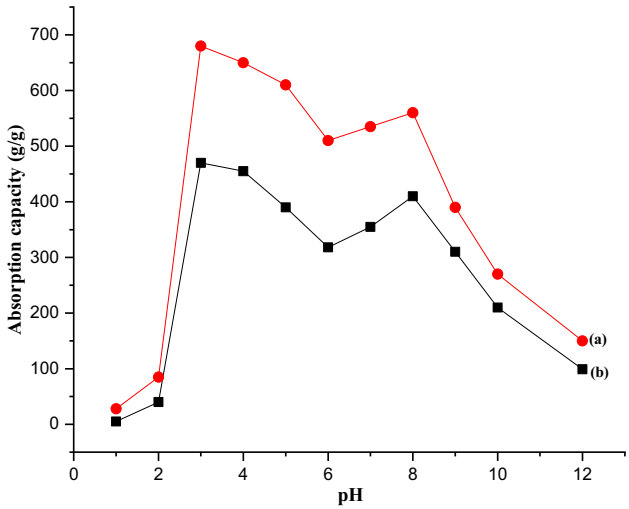

Fig. 6 Effect of environmental pH on water absorbency of (*a*) CTS-g-P(AA-*co*-AM)/BT, (*b*) CTS-g-P(AA-*co*-AM)

study, no buffer solutions are used to avoid the influence of ionic strength on water absorbency. Only solutions of HCl (pH 1.0) and NaOH (pH 13.0) are used to adjust the pH values of the studied solutions.

According to Fig. 6, the two sharp swelling capacity changes around pH values of 3 and 8 can be linked to high repulsion of ammonium groups $–NH_3^+$ in acidic media and carboxylate groups $–COO^-$ in basic media. However, at very acidic conditions (pH ≤ 2), a screening effect of counter ions, such as. Cl^-, shields the positive charge of the ammonium cations and prevents the electrostatic repulsion inside the hydrogel network. Consequently, a huge decrease in swelling capacity is observed. The decrease in water absorbency in the interval of pH between 4 and 6 may be attributed to the formation of additional crosslinking in the network by hydrogen bonds between amines and carboxylic acids groups. The effect of the ionization of carboxylic acids starts to take place when pH is above 6. By increasing the pH, the electrostatic repulsion between carboxylate groups favors the enhancement of water absorbency. However, when pH values are above 9, a screening effect of the counter ions (Na^+) intervenes again and limits the swelling [40].

The swelling kinetics of CTS-g-P(AA-*co*-AM) and its composite with basalt at different pH values is also investigated (Figs. 6S, 7). It is readily proved that the swelling kinetics of the hydrogel and its composite with basalt are dependent on the pH values of the swelling medium.

The effect of different pH values on the swelling kinetics is studied using Schott's pseudo second-order swelling kinetics model [50]:

$$\frac{t}{S_w} = \frac{1}{k_{it}} + \frac{1}{S_\infty} t \tag{6}$$

where S_w is the swelling ratio at time t, S_∞ is the theoretical equilibrium swelling ratio and k_{it} is the initial swelling rate constant.

From Figs. 6S and 7, the swelling kinetic parameters (k_{it} and S_∞) in various pH solutions using the Schott's pseudo second order kinetics model are calculated in Table 3. Since, the plots of the average swelling rate $\frac{t}{S_\infty}$ versus time t are straight lines($R^2 > 0.997$), it suggests that the swelling process follows a pseudo second-order swelling kinetic model, Fig. 7S(a, b). The k_{it} and S_∞ values are estimated from the slope and intercept of the fitted straight lines [51].

From Table 3, it can easily be seen that S_{eq} and S_∞ are almost the same, indicating that 2 h are sufficient for both hydrogels to attain 95% of their theoretical equilibrium absorbencies. On the other hand, k_{it} values have the same trend as S_∞ with the changes of pH values.

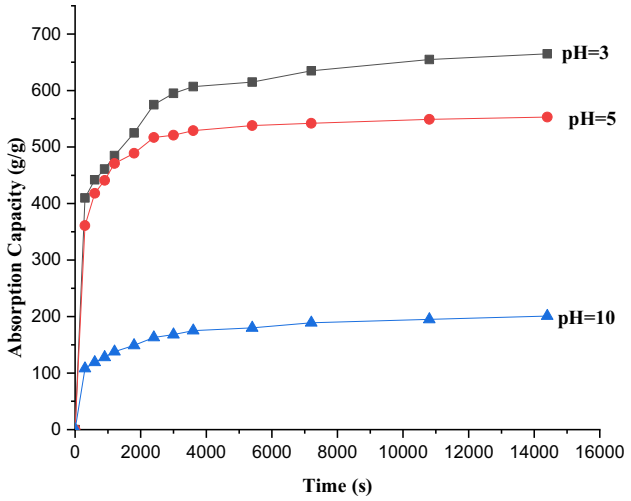

Fig. 7 Swelling kinetics at different pH values of CTS-g-P(AA-*co*-AM)/BT

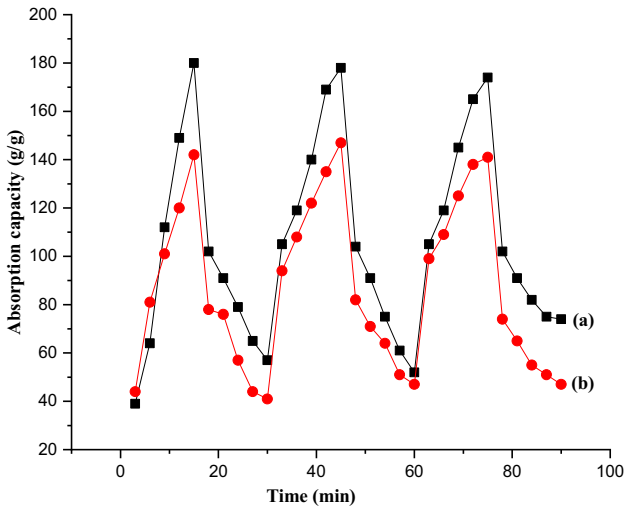

Fig. 8 Swelling-deswelling behavior of (*a*) CTS-g-P(AA-*co*-AM)/BT, (*b*) CTS-g-P(AA-*co*-AM) between pHs 10.0 and 3.0, respectively. The time interval between the pH changes is 15 min. The ascending portion of the curve is for pH 3 and the descending one is for pH 10

As CTS-g-P(AA-*co*-AM) and its composite with basalt show swelling behaviors dependent on pH values, the reversibility of their swelling in with different pH values is investigated. Two pH values are chosen: 3.0 and 10.0. Figure 8 depicts a stepwise reversible swelling change of the CTS-g-P(AA-*co*-AM) and its composite with basalt at 25 °C when changing pH value between 3.0 and 10.0. The time interval between the pH changes is 15 min. At pH 3.0, both the hydrogel and its composite with basalt swell due to ammonium–ammonium repulsive electrostatic forces, while at pH 10.0 they quickly collapse due to the screening effect of Na^+ ions. This acute swelling-deswelling behavior of CTS-g-P(AA-*co*-AM) and its composite with basalt makes them suitable candidates for controlled releasing systems and agricultural applications [52].

CTS-g-P(AA-*co*-AM)/BT as a Soil Conditioner

Eggplant (*Solanum melongena*) was taken as a model to study the role of the composite hydrogel CTS-g-P(AA-*co*-AM)/BT as a soil conditioner. It was chosen over the hydrogel CTS-g-P(AA-*co*-AM) since it is more cost-effective and has higher absorption capacity, better swelling rate and greater water retention. Moreover, it has the potentiality to provide the plant with nutrients [53, 54]. The duration of the experiment was 4 months. It started at the beginning of July and finished at the end of October. The experiment comprises two treatments with five replications for each one. The first treatment used the hydrogel as a soil ameliorant, while the second one was left as a control with no added hydrogel. The weight percentage of the dry hydrogel in the soil was 0.1% wt. The hydrogel was added to the soil after being immersed in water for 24 h.

Figure 9 shows that plants with hydrogel and without it at the end of the forth month, whereas, Fig. 10 exhibits the whole plants after being extracted from the soil. The results prove that the use of composite hydrogel increases the yield. This increase in yield can be attributed to the fact that the soil was wet for a longer time which enhanced the microbial activity as well as reduced the fruit drop owing to water stress. With respect to the growth of plant, an appreciable increase in the growth when composite hydrogel was used in comparison to control. It was also observed that hydrogel composite was able to retain available water for the plant up to 2 weeks after irrigation.

The treatment with the hydrogel exhibits an increment in yield of 85.7%, an increment in plant length of 27%, and an increment in number of leaves of 196% in comparison with the control one.

Table 3 Swelling kinetic parameters (k_{it} and S_∞) in various pH solutions of CTS-g-P(AA-*co*-AM) and CTS-g-P(AA-*co*-AM)/BT

pH	10	5	3	10	5	3
	CTS-g-P(AA-*co*-AM)			CTS-g-P(AA-*co*-AM)/BT		
k_{it} g/(g s)	0.075	1.02	1.15	0.415	2.960	2.267
S_∞ g/g	99	360	526	208	559	610
S_{eq} g/g	92	355	489	201	553	603

Fig. 9 The model plant without hydrogel as control (left) and with composite hydrogel (right) after 4 months

Fig. 10 The whole model plant with the roots without hydrogel as a control (left) and with composite hydrogel (right) after 4 months

Conclusion

The preparation of a new environmentally friendly superabsorbent composite, using a renewable and biodegradable substrate of chitosan, and a soil conditioner based on ground basaltic rock, is succeeded. Chitosan and basalt are both abundant and cost-effective. Their quantities were optimized to get the maximum absorbency with accepted gel strength. The mass ratio of chitosan and ground basalt to monomers is as high as 1:3. The synthesis of the current composite hydrogel CTS-g-P(AA-*co*-AM)/BT was performed by free-radical graft copolymerization under microwave irradiation. FTIR and XRD analyses confirmed that the successful synthesis. The new hydrogel exhibits excellent pH-sensitivity, good pH-dependent swelling

reversibility and high water retention capability, making it a promising water-saving material for agricultural and horticultural applications.

References

1. Straaten P (2006) Ann Braz Acad Sci 78:731
2. Magalhães M, Neto M, Bezerra J, Feitosa (2013) J Braz Chem Soc 24:304
3. M.Queirós M, Bezerra J, Feitosa (2017) J Braz Chem Soc 28:2004
4. Kalaleh HA, Tally M, Atassi Y (2015) Polym Sci Ser B 57:750
5. Puoci F, Iemma F, Spizzirri UG, Girillo G, Curcio M, Picci N (2008) Am J Agric Biol Sci 3:299
6. Dubrovskii SA, Afanas'eva MV, Lagutina MA, Kazanskii KS (1990) Polym Bull 24:107
7. Shi Y, Xue Z, Wang X, Wang L, Wang A (2013) Polym Bull 70:1163
8. Cheng W, Hu X, Xie J, Zhao Y (2017) Fuel 210:826
9. Ekebafe LO, Ogbeifun DE, Okieimen FE (2011) Biokemistri 23:81
10. Raju KM, Raju P, Mohan YM (2001) J Appl Polym Sci 85:1795
11. Qin S, Wu Z, Rasool A, Li C (2012) J Appl Polym Sci 126:1687
12. Waham L, Shahrir H, Akos I (2011) Polym Plast Technol Eng 50:1475
13. Hedrick RM, Mowry DT (1952) Soil Sci 73:427
14. Tally M, Atassi Y (2016) Polym Bull 22:1
15. Abd El-Rehim HA (2006) J Appl Polym Sci 101:3572
16. He G, Ke W, Chen X, Kong Y, Zheng H, Yin Y, Cai W (2017) React Funct Polym 111:14
17. Li A, Liu R, Wang A (2005) J Appl Polym Sci 98:1351
18. Li A, Liu R, Wang A (2017) R Soc Open Sci 4:170829
19. Liu Y, Zheng Y, Wang A (2010) J Environ Sci 22:486
20. Zhang J, Wang Q, Wang A (2007) Carbohydr Polym 68:367
21. Zhang J, Wang L, Wang A (2007) Ind Eng Chem Res 46:2497
22. Barak P, Chen Y, Singer A (1983) Plant Soil 73:155
23. Leonardos OH, Fyfe WS, Kronberg BI (1987) Chem Geol 60:361
24. Von Fragstein P, Pertl W, Vogtmann H (1988) J Plant Nutr Soil Sci 151:141
25. Hamed F, Ozogul J, Regenstein (2016) Trends Food Sci Technol 48:40
26. Zohuriaan-Mehr MJ, Kabiri K (2008) J Iran Polym 17:451
27. El-Sayed M, Sorour M, Abdelmoneem N, Talaat H, Shalaan H, Elmarsafy S (2011) J World Appl Sci 13:360
28. Ghasemzadeh H, Ghanaat F (2014) J Polym Res 21:355
29. Ferfera-harrar H, Aiouaz N, Dairi N, Hadj-Hamou A (2014) J Appl Polym Sci 39747:1
30. Rashidzadeh A, Olad A, Salari D, Reyhanitabar A (2014) J Polym Res 21:344
31. Huang M, Shen X, Sheng Y, Fang Y (2005) Int J Biol Macromol 36:98
32. Bao Y, Ma J, Li N (2011) J Carbohydr Polym 84:76
33. Feng I, Guo X, Qiu K (1988) MakromolekulChem 189:77
34. Gharekhani H, Olad A, Mirmohseni A, Bybordi A (2017) Carbohydr Polym 168:1
35. Anda M, Shamshuddin J, Fauziah C, Omar SR (2009) Soil Sci 174:264
36. Wang L, Zhang J, Wang A (2008) Colloids Surf A Physicochem Eng Asp 322:47
37. El-Shahate M, Saraya I (2014) Constr Build Mater 72:104
38. Spagnol FHA, Rodrigues AGVC., Neto AGB, Pereira AR, Fajardo E, Radovanovic AF, Rubira EC, Muniz (2012) J Eur Polym 48:454
39. Kalaleh HA, Tally M, Atassi Y (2013) Res Rev Polym 4:145
40. Mahdavinia GR, Pourjavadi A, Hosseinzadeh H, Zohuriaan MJ (2004) J Eur Polym 40:1399
41. Kumar S, Koh J (2012) Int J Mol Sci 13:6102
42. Bashir S, Teo Y, Naeem S, Ramesh S, Ramesh K (2017) PLoS ONE. https://doi.org/10.1371/journal.pone.0179250
43. Zhang Q, Hu XM, Wu MY, Zhao Y, Yu C (2018) J Appl Polym Sci 135:46460
44. Lim DW, Yoon KJ, Ko SW (2000) J Appl Polym Sci 78:2525
45. Ganji F, Vasheghani-Farahani S, Vasheghani-Farahani E (2010) Iran Polym J 19:375
46. Kabiri K, Omidian H, Hashemi SA, Zohuriaan-Mehr MJ (2003) Euro Polym J 39:1341
47. Kalaleh H, Atassi A (2018) J Mater Environ Sci 9:955
48. Hu ZX, Hu XM, Cheng WM, Lu W (2018) High Perform Polym. https://doi.org/10.1177/0954008318758489
49. Lanthong P, Kiatkamjornwong S (2006) Carbodydr Polym 66:229
50. Schott H (1992) J Macromol Sci 31:1
51. Wang, Wang L, Zhang J, Wang A (2011) Desalination 266:33
52. Hosseinzadeh H, Sadeghzadeh M, Badazadeh M (2011) J Biomater Nanobiotechnol 2:311
53. Wang W, Wang A (2009) J Appl Polym Sci 112:2102
54. Wen P, Wu Z, He Y, Ye B, Han Y, Wang J, Guan X (2016) ACS Sustain Chem Eng 4:6572